Large enhancement of third-harmonic generation induced by coupled gap solitons in $\chi^{(3)}$ nonlinear photonic crystals

Ping Xie and Zhao-Qing Zhang
Department of Physics and Institute of Nano Science and Technology (INST), The Hong Kong University of Science and Technology, Clear Water Bay, Hong Kong, China
(Received 15 September 2004; published 23 February 2005)

It is shown that, in a $\chi^{(3)}$ nonlinear photonic crystal, the third-harmonic conversion efficiency can be enhanced by about three orders of magnitude via the formation of self-organized localized states inside the gaps as compared with that in a bulk medium of the same length with a perfect phase-matching condition. These localized states contain both the fundamental and third-harmonic frequencies located in different gaps. Their existence is a result of both the Kerr effect and the large energy transfer between fundamental and third-harmonic waves.

DOI: 10.1103/PhysRevE.71.026610 PACS number(s): 42.70.Qs, 42.65.Tg, 63.20.Pw

Recently, great interest has been devoted to nonlinear photonic crystals (NPCs) [1]. The combination of photonic crystals and nonlinear optics has opened up a new area of research for both science and application. For example, in a $\chi^{(2)}$ NPC, it has been shown that the efficiency of second-harmonic (SH) generation can be enhanced by use of the simultaneous availability of field localization at the band edge and a good phase-matching condition [2]. The gap solitons and two-color gap solitons with fundamental and SH frequencies located in different gaps have been found in $\chi^{(2)}$ NPCs [3–7]. For $\chi^{(3)}$ NPCs, two different nonlinear effects have been studied: Kerr nonlinearity and third-harmonic (TH) generation. For TH generation, Martemyanov *et al.* have recently studied the enhancement of TH conversion efficiency by making use of the field localization of the band-edge state or the defect state [8]. Markowicz *et al.* have experimentally demonstrated the enhancement by making use of phase matching provided by the periodicity of photonic crystals [9]. For Kerr nonlinearity, by changing the light intensity at a frequency in the pass band, it has been shown that the band-edge frequency can be dynamically tuned [10]. When the frequency is in the gap, the self-organized localized state (SOLS), which is usually associate with gap soliton, can be formed [11–19]. However all the SOLS found previously in $\chi^{(3)}$ NPCs are derived from the pure Kerr effect by ignoring the influence of the third-harmonic waves generated due to $\chi^{(3)}$ nonlinearity. This is valid only when the phase-matching condition does not hold.

In this work, we show that the interplay between two different $\chi^{(3)}$ effects in a NPC can give rise to interesting phenomena with potential applications. Specifically, we consider the situation in which the phase-matching condition holds due to the periodicity of the photonic crystals and the nonlinear interaction between the TH waves generated, and the fundamental waves via Kerr effect cannot be ignored. We find that, through the formation of a coupled localized state (CLS) with the fundamental and the TH frequencies located in different gaps coupled, the TH conversion efficiency can be enhanced significantly, e.g., by about three orders of magnitude, as compared with that in a bulk medium of the same length with a perfect phase-matching condition.

Consider a one-dimensional (1D) NPC with N unit cells. One layer in each unit cell is linear, with the refractive index n_1 and width l_1. The other layer is nonlinear, with the weak-field refractive index n_2 and a third-order nonlinear susceptibility $\chi^{(3)}$. The width of the nonlinear layer is l_2. A pump wave $\tilde{E}_F$ of frequency ω is incident normally upon the sample along the z axis. When the phase-matching condition is good, a TH wave $\tilde{E}_H$ can be generated via the $\chi^{(3)}$ nonlinearity. We represent the fundamental and the TH waves by $\tilde{E}_F(z,t)=E_F(z)e^{-i\omega t}+\text{c.c.}$ and $\tilde{E}_H(z,t)=E_H(z)e^{-3i\omega t}+\text{c.c.}$, where $E_\alpha(z,t)=E_\alpha^+(z)+E_\alpha^-(z)$ $(\alpha=F,H)$ and $E_\alpha^\pm(z)=A_\alpha^\pm(z)e^{\pm ik_\alpha z}$. Here E_α^+ and E_α^- denote the forward and backward propagating components, respectively. From the nonlinear polarization $\tilde{P}(z,t)=\chi^{(3)}\tilde{E}(z,t)^3$, where $\tilde{E}(z,t)=\tilde{E}_F(z,t)+\tilde{E}_H(z,t)$, we have $\tilde{P}_F(z,t)=\chi^{(3)}[3(|E_F|^2+2|E_H|^2)E_Fe^{-i\omega t}+3E_F^{*2}E_He^{-i\omega t}+\text{c.c.}]$ and $\tilde{P}_H(z,t)=\chi^{(3)}\times[3(2|E_F|^2+|E_H|^2)E_He^{-3i\omega t}+E_F^3e^{-3i\omega t}+\text{c.c.}]$. Substituting $\tilde{E}_\alpha$ and $\tilde{P}_\alpha$ into $\nabla^2\tilde{E}_\alpha-[\varepsilon(\omega_\alpha)/c^2](\partial^2\tilde{E}_\alpha/\partial t^2)=(4\pi/c^2)\times(\partial^2/\partial t^2)\tilde{P}_\alpha$ and making the slowly-varying-amplitude approximation, we obtain

$$\frac{dA_F^\pm}{dz}=\pm i\kappa_F A_F^\pm \pm i\gamma_F A_F^{\pm *2}A_H^\pm e^{\pm i\Delta kz}, \tag{1a}$$

$$\frac{dA_H^\pm}{dz}=\pm i\kappa_H A_H^\pm \pm i\gamma_H A_F^{\pm 3}e^{\mp i\Delta kz}, \tag{1b}$$

where

$$\begin{aligned}\gamma_F&=6\pi\omega\chi^{(3)}/n(\omega)c,\\ \gamma_H&=6\pi\omega\chi^{(3)}/n(3\omega)c,\\ \kappa_F&=\gamma_F(|E_F^++E_F^-|^2+2|E_H^++E_H^-|^2),\\ \kappa_H&=3\gamma_H(2|E_F^++E_F^-|^2+|E_H^++E_H^-|^2),\end{aligned} \tag{2}$$

and $\Delta k=k_H-3k_F$ produces phase mismatch in the case of weak fields. Notice that the second terms in the right-hand

side of Eqs. (1a) and (1b) are responsible for the TH conversion; whereas the first terms induce the self-phase and cross-phase modulations. Letting $A_\alpha^\pm = A_\alpha^{\pm\prime} e^{\pm i\kappa_\alpha z}$, we re-write Eq. (1) in the following form:

$$\frac{dA_F^{\pm\prime}}{dz} = \pm i\gamma_F \kappa_c^{\pm *} A_H^{\pm\prime} e^{\pm i\Delta k' z}, \tag{3a}$$

$$\frac{dA_H^{\pm\prime}}{dz} = \pm i\gamma_H \kappa_c^{\pm} A_F^{\pm\prime} e^{\mp i\Delta k' z}, \tag{3b}$$

where

$$\kappa_c^\pm = A_F^{\pm\prime 2}$$

and

$$\Delta k' = (k_H - 3k_F) + (\kappa_H - 3\kappa_F). \tag{4}$$

$\Delta k'$ in Eq. (4) produces phase mismatch in the case of strong fields. To solve Eq. (3) we divide each nonlinear layer into M sublayers and assume values of κ_F, κ_H, and $\kappa_c^\pm$ to be constant and equal to their mean values in each sublayer [18,19]. In our calculations, M is taken so that a convergent result is reached. Solving Eq. (3) in each sublayer and using the continuity of both E and the derivative of E at the interface of two sublayers, we finally obtain the following relation:

$$\begin{bmatrix} E_F^+(l_{s,i}) \\ E_F^-(l_{s,i}) \\ E_H^+(l_{s,i}) \\ E_H^-(l_{s,i}) \end{bmatrix} = \tau^{(s,i)} \begin{bmatrix} E_F^+(l_{s,i-1}) \\ E_F^-(l_{s,i-1}) \\ E_H^+(l_{s,i-1}) \\ E_H^-(l_{s,i-1}) \end{bmatrix}, \tag{5a}$$

$$\tau^{(s,i)} = \frac{1}{2}\begin{bmatrix} (1+a_F)t_{11}^+ & (1-a_F)t_{11}^+ & (1+a_H)t_{12}^+ & (1-a_H)t_{12}^+ \\ (1-a_F)t_{11}^- & (1+a_F)t_{11}^- & (1-a_H)t_{12}^- & (1+a_H)t_{12}^- \\ (1+a_F)t_{21}^+ & (1-a_F)t_{21}^+ & (1+a_H)t_{22}^+ & (1-a_H)t_{22}^+ \\ (1-a_F)t_{21}^- & (1+a_F)t_{21}^- & (1-a_H)t_{22}^- & (1+a_H)t_{22}^- \end{bmatrix}, \tag{5b}$$

where $l_{s,i}$ is the width of the sublayer i in the s-layer, $a_F = n^{(s,i-1)}(\omega)/n^{(s,i)}(\omega)$ and $a_H = n^{(s,i-1)}(3\omega)/n^{(s,i)}(3\omega)$, with $n^{(s,i)}$ the refractive index of the sublayer,

$$t_{11}^\pm = \left[\frac{\delta_0^\pm + \Delta k'}{2\delta_0^\pm}\exp\left(\mp i\frac{\delta_0^\pm - \Delta k'}{2}l_{s,i}\right) + \frac{\delta_0^\pm - \Delta k'}{2\delta_0^\pm}\exp\left(\pm i\frac{\delta_0^\pm + \Delta k'}{2}l_{s,i}\right)\right]\exp[\pm i(k_F + \kappa_F)l_{s,i}],$$

$$t_{12}^\pm = \frac{\gamma_F \kappa_c^{\pm *}}{\delta_0^\pm}\left[\exp\left(\pm i\frac{\delta_0^\pm + \Delta k'}{2}l_{s,i}\right) - \exp\left(\mp i\frac{\delta_0^\pm - \Delta k'}{2}l_{s,i}\right)\right]\exp[\pm i(k_F + \kappa_F)l_{s,i}],$$

$$t_{21}^\pm = \frac{\gamma_H \gamma_c^\pm}{\delta_0^\pm}\left[\exp\left(\pm i\frac{\delta_0^\pm - \Delta k'}{2}l_{s,i}\right) - \exp\left(\mp i\frac{\delta_0^\pm + \Delta k'}{2}l_{s,i}\right)\right]\exp[\pm i(k_H + \kappa_H)l_{s,i}],$$

$$t_{22}^\pm = \left[\frac{\delta_0^\pm + \Delta k'}{2\delta_0^\pm}\exp\left(\pm i\frac{\delta_0^\pm - \Delta k'}{2}l_{s,i}\right) + \frac{\delta_0^\pm - \Delta k'}{2\delta_0^\pm}\exp\left(\mp i\frac{\delta_0^\pm + \Delta k'}{2}l_{s,i}\right)\right]\exp[\pm i(k_H + \kappa_H)l_{s,i}],$$

with $\delta_0^\pm = \sqrt{(\Delta k')^2 + 4\gamma_F\gamma_H|\kappa_c^\pm|^2}$. Note that it is through relation (5), which couples the forward and backward propagating waves. For the linear layer, we take $\chi^{(3)}=0$ and $M=1$. From the products of these matrices, $T = \Pi_{i=1}^{N(M+1)}\tau^{(s,i)}$, we obtain the amplitudes of the fundamental and TH waves at $z=0$ as $E_F^-(0) = (T_{21}T_{44} - T_{24}T_{41})/(T_{24}T_{42} - T_{22}T_{44})E_F^+(0)$ and $E_H^-(0) = (T_{22}T_{41} - T_{21}T_{42})/(T_{24}T_{42} - T_{22}T_{44})E_F^+(0)$, respectively, and at $z=L$ as $E_F^+(L) = T_{11}E_F^+(0) + T_{12}E_F^-(0) + T_{14}E_H^-(0)$ and $E_H^+(L) = T_{31}E_F^+(0) + T_{32}E_F^-(0) + T_{34}E_H^-(0)$, respectively.

The above equations are solved numerically by using an iterative procedure [18,19]. We emphasize that all the solutions presented in this work are stable. In fact, if a solution is not stable in time, i.e., the solution is not a fixed attractor, the iterative procedure will never be convergent to a limiting result. For calculations, we use a 1D model NPC with $N=18$ unit cells, with $n_1=1$, $n_2^2(\lambda) = 8.340\,96 + 0.145\,40/(\lambda^2 - 0.239\,79^2) + 3.239\,24/(\lambda^2/36.525^2 - 1)$ [20], where $\lambda = 2\pi c/\omega$ is the wavelength in vacuum (in units of μm), $l_1 = 0.112$ μm, and $l_2 = 0.10$ μm. As we will see below, such choices of n_1, n_2, l_1, and l_2 can give a near phase matching for TH conversion when the fundamental wavelength λ_F is chosen near the high-wavelength band edge of the first gap. It should be pointed out that the other choices of n_1, n_2, l_1, and l_2 will give results similar to those presented in this work, provided that the values of l_1 and l_2 are adjusted so that they give a near phase matching for TH conversion when the fundamental wavelength λ_F is chosen near the high-wavelength band edge of the first gap and the corresponding TH wavelength λ_H is located near that of another gap. Thus, the general features obtained in this work should not be limited to the specific model parameters we have chosen above. As for third-order susceptibility, we choose a dimensionless $\chi^{(3)} = -10^{-4}$ for calculations. Therefore, the corresponding fields appearing in our calculations are also dimensionless. The conversions of $\chi^{(3)} = -10^{-4}$ and the fields used in our calculations to those in a realistic situation will be discussed at the end of the work.

The transmission spectrum of the linear model sample is shown in Fig. 1(a) and the corresponding effective index of refraction n_{eff} is shown in Fig. 1(b) by a solid line, where the dotted line is for $n_2(\lambda)$. The wavelength at the high-wavelength band edge of the first gap is $\lambda_1 = 901.6$ nm and that of the third gap is $\lambda_3 = 298.95$ nm. From Fig. 1(b) we note that, for the fundamental wavelength λ_F chosen near λ_1, the TH conversion has a good phase-matching condition. As is known, the $\chi^{(3)}$ nonlinearity can induce the shift of the band edge or the formation of gap solitons for the fundamental waves [10–19] via the first term on the r.h.s. of Eq. (1a). Thus, in order to take advantage of their localized fields to enhance the TH conversion, which is represented by the second term on the r.h.s. of Eq. (1b) or the r.h.s. term of Eq. (3b), we should choose λ_F slightly smaller than λ_1 for the

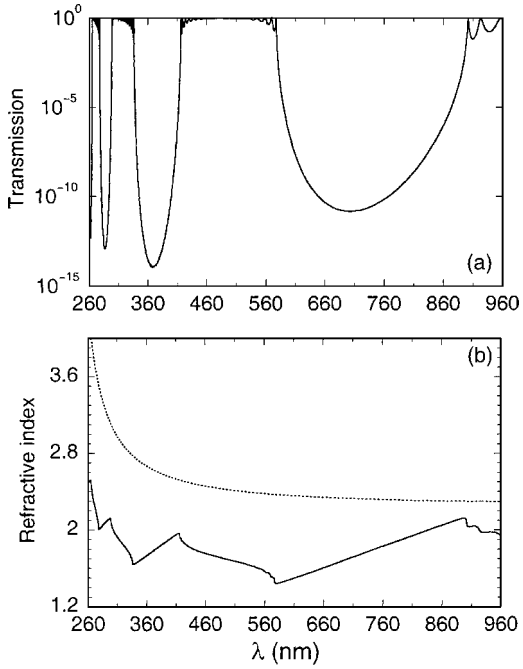

FIG. 1. (a) Transmission spectrum of the linear sample. (b) Effective refractive-index dispersion of the linear sample (solid curve) and the weak-field refractive-index dispersion of the nonlinear layer (dotted curve).

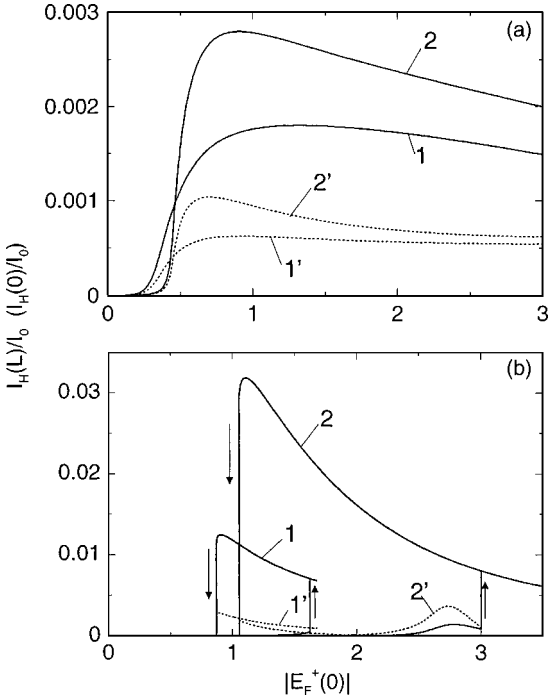

FIG. 2. Third-harmonic conversion efficiencies, $I_H(L)/I_0$ (solid lines) and $I_H(0)/I_0$ (dotted lines), versus the incident amplitude $|E_1^+(0)|$, where $I_H(L)=|E_H^+(L)|^2$, $I_H(0)=|E_H^-(0)|^2$, and $I_0=|E_F^+(0)|^2$. (a) Curves 1 and 1′ for fundamental wavelength $\lambda_F=901$ nm; curves 2 and 2′ for $\lambda_F=900.5$ nm. (b) Curves 1 and 1′ for $\lambda_F=898$ nm; curves 2 and 2′ for $\lambda_F=896$ nm.

negative $\chi^{(3)}$. In Fig. 2 we show some typical results of output TH intensities $I_H(L)=|E_H^+(L)|^2$ and $I_H(0)=|E_H^-(0)|^2$ for various λ_F. When λ_F is very near λ_1, the $\chi^{(3)}$ nonlinearity induces the shift of the band edge. The maximum TH conversion in Fig. 2(a) occurs at about the input amplitude that shifts the band edge to λ_F. As λ_F is moved away from λ_1, the maximum TH conversion efficiency is increased. This occurs for two reasons. First, as λ_F moved away from λ_1 the band-edge state becomes more localized and thus the fundamental field inside the sample increases. Second, both the increase of the localized field (nonlinear effect) and the move of λ_F (λ_H) (linear effect) give rise to a decrease in the phase mismatch condition $|\Delta k'|$ in Eq. (4). When λ_F is further moved into the gap, the formation of gap soliton for λ_F occurs. This leads to the bistability of the fundamental field inside the sample. The bistable output for the TH wave is shown in Fig. 2(b). Compared with Fig. 2(a), Fig. 2(b) shows clearly the enhancement of TH conversion via the formation of gap solitons for λ_F. It should be pointed out that although λ_F in Fig. 2(b) ($\lambda_F=898$ nm and 896 nm) is now inside the first gap, the TH waves ($\lambda_H=299.3$ nm for curves 1 and 1′ and 298.7 nm for curves 2 and 2′) are still close to the high-wavelength band edge of the third gap.

When λ_F is further moved into the gap and the corresponding λ_H is now pushed into the third gap, the tristability behavior occurs. Figures 3(a) and 3(b) show the two typical results of $I_H(L)$ and $I_H(0)$ for $\lambda_F=892.5$ nm ($\lambda_H=297.5$ nm) and $\lambda_F=891$ nm ($\lambda_H=297$ nm), respectively. We note that there exists an optimal wavelength at $\lambda_F\approx 892.5$ nm where the sum of $I_H(L)/I_0$ and $I_H(0)/I_0$ reaches a maximum. This corresponds to the situation in which the induced localized state gives rise to a nearly perfect phase-match condition; i.e., $|\Delta k'|\approx 0$ in Eq. (4). Note also that the energy-transfer efficiency shown in Fig. 3(a) is about 43% at point A', which is about three orders of magnitude larger than that in a bulk medium of the same length, i.e., $L=(l_1+l_2)N=3.816$ μm, with a perfect phase-match condition. In Fig. 3(c) we show the corresponding $I_F(L)=|E_F^+(L)|^2$ and $I_F(0)=|E_F^-(0)|^2$ for $\lambda_F=891$ nm. We note that the intensity distributions for λ_F at points A and B are both localized with single envelope. The state at point B is derived from the gap soliton found previously when there is no TH conversion [11–18]. The transmission behavior of this case is shown in the inset of Fig. 3(c), where there exists only one single-envelope localized state at point C [11], which has perfect transmission at the same value of $|E_F^+(0)|$ as that of point B. In the presence of TH conversion, the transmission at B is slightly smaller than unity due to a small amount of energy transfer from fundamental waves to TH waves, as shown in the corresponding point B' in Fig. 3(b). In addition to B, there exists another stable localized state at points D and D' at the same $|E_F^+(0)|$, which has a much larger TH intensity. The points A and A' emerging from D and D' represent the same branch of stable localized state, but with wave functions symmetric to the center of the sample. Since λ_H is now located inside the third gap, the intensity distribution for λ_H is also localized. Thus, the new state at A and A' represents a coupled localized state (CLS) containing both fundamental and TH frequencies located in different gaps.

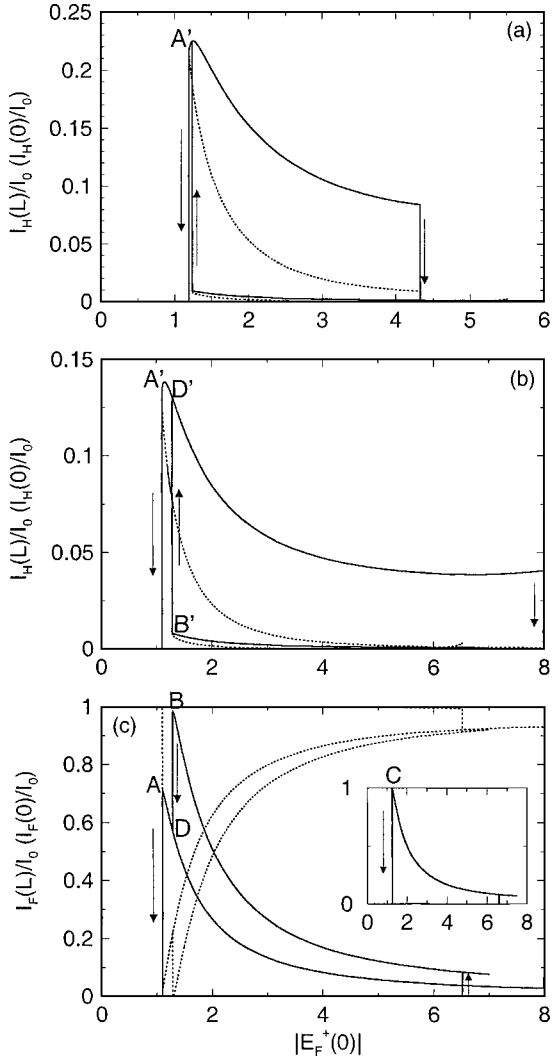

FIG. 3. Third-harmonic conversion efficiencies, $I_H(L)/I_0$ (solid lines) and $I_H(0)/I_0$ (dotted lines), versus the incident amplitude $|E_1^+(0)|$ for $\lambda_F=892.5$ nm (a) and $\lambda_F=891$ nm (b). (c) Transmission $I_F(L)/I_0$ (solid line) and reflection $I_F(0)/I_0$ (dotted line) versus $|E_1^+(0)|$ for $\lambda_F=891$ nm. $I_H(L)=|E_H^+(L)|^2$, $I_H(0)=|E_H^-(0)|^2$, $I_F(L)=|E_F^+(L)|^2$, $I_F(0)=|E_F^-(0)|^2$, and $I_0=|E_F^+(0)|^2$. The inset shows the transmission $I_F(L)/I_0$ of the beam with $\lambda_F=891$ nm without the third-harmonic conversion.

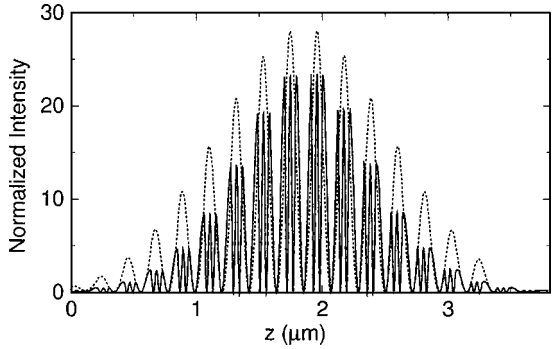

FIG. 4. Intensity distributions normalized by I_0 for $\lambda_F=892.5$ nm (dotted curve) and $\lambda_H=297.5$ nm (solid curve) at point A' of Fig. 3(a).

In Fig. 4, we show the CLS of λ_F and λ_H for the point A' in Fig. 3(a), where maximum TH conversion occurs. Figure 4 shows clearly two localized distributions for λ_F and λ_H, both symmetric to the center of the sample. Their magnitudes are comparable, indicating significant energy exchange between λ_F and λ_H occurring in this new state. Its existence greatly enhances the TH conversion. This is in contrast with the state at points B and B'. Although their intensity distributions are also localized for both λ_F and λ_H, the intensity for λ_H is only about 3% of that for λ_F. It should be mentioned that, similar to the gap soliton at point C in the inset of Fig. 3(c), the shape and size of the CLS at point A' is also insensitive to the sample thickness. This can be understood as the fields outside the core regions of the CLS for both λ_F and λ_H are exponentially small and their contribution to the energy exchange is negligible. The formation of this CLS is a result of both Kerr effect and large energy exchange between λ_F and λ_H. The Kerr effect is represented by the first terms on the r.h.s. of Eqs. (1a) and (1b). These terms change only the phases of λ_F and λ_H through both self-phase and cross-phase modulations. However, the second terms on the r.h.s. of Eqs. (1a) and (1b) induce also the energy exchanges between λ_F and λ_H. Such energy exchange in $\chi^{(3)}$ NPCs was first addressed in Ref. 21. It should be mentioned that the formation mechanism of this CLS is different from the two-color gap soliton found in $\chi^{(2)}$ NPCs [3–7]. In $\chi^{(2)}$ NPCs, the formation of two-color gap soliton arises from the terms that are equivalent to the second terms on the r.h.s. of Eqs. (1a) and (1b), and there exists no genuine Kerr effect. In the case of a very large phase mismatch, the $\chi^{(2)}$ nonlinearity can be reduced to the Kerr-equivalent limit through cascading $\chi^{(2)}$ effects [3–7]. However, in this case, there exists almost no energy conversion from the fundamental to the SH waves. The presence of the Kerr effect in the first terms on the r.h.s. of Eqs. (1a) and (1b) is crucial to obtain the CLS shown in this work. In fact, we cannot obtain this CLS if the first terms in Eqs. (1a) and (1b) are dropped. We also mention that the CLS presented in this work is also different from the multi-frequency gap soliton (MFGS) found in Ref. [19]. The difference is that the formation of a MFGS is due to synergic spatial modulations of dielectric constant arising from intensity distributions at different frequencies. That is, a MFGS is due solely to the Kerr effect and there exists no energy exchange between any two frequency components.

Finally, we give an estimate of the source power required to observe the phenomena shown in this work. If the units of field are chosen as statvolt/cm, $\chi^{(3)}=-10^{-4}$ taken in our calculation corresponds to $\chi^{(3)}=-10^{-4}$ esu, and the value of $|E_F^+(0)|=1-7$ in Figs. 2 and 3 then gives $|E_F^+(0)|=1-7$ statvolt/cm, which corresponds to a laser power of $I=(1/2)c\varepsilon_0|E_F^+(0)|^2\approx 180-8820$ W/cm^2. Thus, for a more realistic number $\chi^{(3)}=-10^{-9}$ esu, the value of $|E_F^+(0)|=1-7$ corresponds to a laser power of $I\approx 18-882$ MW/cm^2, which is attainable in practice.

In conclusion, we demonstrate that the TH conversion efficiency can be enhanced by about three orders of magnitude

through the formation of a coupled localized state in $\chi^{(3)}$ NPCs as compared with that in a bulk medium of the same length with a perfect phase-matching condition. This localized state couples the fundamental and TH waves located in different gaps. Its existence is a result of both Kerr effect and large energy transfer between fundamental and TH waves through $\chi^{(3)}$ nonlinearity.

This work was supported by Hong Kong RGC Grant No. 605804.

[1] See, for example, C. M. Bowden and A. M. Zheltikov, J. Opt. Soc. Am. B **19**, 2046 (2002), and references therein.
[2] M. Scalora *et al.*, Phys. Rev. A **56**, 3166 (1997); Opt. Photonics News **2001**, 38; A. V. Andreev *et al.*, J. Opt. Soc. Am. B **19**, 2083 (2002); A. M. Malvezzi *et al.*, *ibid.* **19**, 2122 (2002).
[3] Y. Kivshar, Phys. Rev. E **51**, 1613 (1995).
[4] C. Conti, S. Trillo, and G. Assanto, Phys. Rev. Lett. **78**, 2341 (1997).
[5] H. He and P. D. Drummond, Phys. Rev. Lett. **78**, 4311 (1997).
[6] C. Conti, S. Trillo, and G. Assanto, Opt. Lett. **22**, 1350 (1998); **23**, 334 (1998); **23**, 1265 (1998).
[7] A. V. Buryak, P. D. Trapani, D. V. Skryabin, and S. Trillo, Phys. Rep. **370**, 63 (2002).
[8] M. G. Martemyanov, T. V. Dolgova, and A. A. Fedyanin, J. Exp. Theor. Phys. **98**, 463 (2004).
[9] P. P. Markowicz *et al.*, Phys. Rev. Lett. **92**, 083903 (2004).
[10] M. Scalora *et al.*, Phys. Rev. Lett. **73**, 1368 (1994); P. Tran, Opt. Lett. **21**, 1138 (1996).
[11] W. Chen and D. L. Mills, Phys. Rev. Lett. **58**, 160 (1987).
[12] D. N. Christodoulides and R. I. Joseph, Phys. Rev. Lett. **62**, 1746 (1990).
[13] C. M. de Sterke and J. E. Sipe, in *Progress in Optics XXXIII*, edited by E. Wolf (Elsevier, Amsterdam, 1994), Chap. III.
[14] S. John and N. Akozbek, Phys. Rev. Lett. **71**, 1168 (1993); Phys. Rev. E **57**, 2287 (1998).
[15] I. V. Barashenkov, D. E. Pelinovsky, and E. V. Zemlyanaya, Phys. Rev. Lett. **80**, 5117 (1998).
[16] A. De Rossi, C. Conti, and S. Trillo, Phys. Rev. Lett. **81**, 85 (1998).
[17] S. F. Mingaleev and Y. S. Kivshar, Phys. Rev. Lett. **86**, 5474 (2001).
[18] P. Xie, Z. Q. Zhang, and X. Zhang, Phys. Rev. E **67**, 026607 (2003); **69**, 036601 (2004).
[19] P. Xie and Z. Q. Zhang, Phys. Rev. Lett. **91**, 213904 (2003).
[20] See, for example, H. H. Li, J. Phys. Chem. Ref. Data **13**, 103 (1984).
[21] C. M. de Sterke and J. E. Sipe, Phys. Rev. A **39**, 5163 (1989).